PNAS RESEARCH ARTICLE | ECOLOGY

Overestimated natural biological nitrogen fixation translates to an exaggerated CO_2 fertilization effect in Earth system models

Sian Kou-Giesbrecht[a,1], Carla R. Reis Ely[b], Steven S. Perakis[c], Cory C. Cleveland[d], Duncan N. L. Menge[e], Sasha C. Reed[f], Benton N. Taylor[g], Sarah A. Batterman[h,i,j], Timothy E. Crews[k], Katherine A. Dynarski[d], Maga Gei[l], Michael J. Gundale[m], David F. Herridge[n], Sarah E. Jovan[o], Mark B. Peoples[p], Johannes Piipponen[q], Emilio Rodríguez-Caballero[r,s], Verity G. Salmon[t], Fiona M. Soper[u], Anika P. Staccone[v], Bettina Weber[w], Christopher A. Williams[x], and Nina Wurzburger[y]

Affiliations are included on p. 10.

Edited by Christopher Field, Stanford University, Stanford, CA; received June 9, 2025; accepted October 22, 2025

CO_2 fertilization of the terrestrial biosphere is limited by nitrogen. Biological nitrogen fixation (BNF) is the dominant natural nitrogen source to the terrestrial biosphere and can alleviate nitrogen limitation but is poorly constrained in Earth system models (ESMs). Here, we compare terrestrial BNF from an ensemble of ESMs of the 6th Coupled Model Intercomparison Project to a new global synthesis of observations across natural and agricultural biomes. We find that compared to observations, ESMs underestimate agricultural BNF but overestimate natural BNF in the present day by over 50%. Natural BNF is overestimated in the most productive ecosystems that contribute most to the terrestrial carbon sink (forests and grasslands). ESMs with different BNF representations yield a range of BNF responses to CO_2 enrichment. Some ESMs with phenomenological representations of BNF predict a natural BNF increase in response to a doubling of CO_2 that aligns with a meta-analysis of CO_2 enrichment experiments (31% increase) but fail to account for the substantial carbon cost of BNF. In contrast, ESMs with mechanistic representations of BNF account for its carbon cost as well as its regulation by nitrogen limitation but overestimate the BNF response to a doubling of CO_2 (135% increase). Overall, all current BNF representations in ESMs fall short of fully capturing its response to rising atmospheric CO_2. Finally, we find a positive correlation between modeled present-day natural BNF and the CO_2 fertilization effect across ESMs, suggesting that overestimated natural BNF translates to an exaggerated CO_2 fertilization effect of approximately 11% in ESMs.

biological nitrogen fixation | CO_2 fertilization | Earth system models

Significance

Earth system models (ESMs) are used to project climate change, which depends in part on how much carbon plants take up. Nitrogen is an essential limiting nutrient to plant growth and carbon uptake, and it is increasingly incorporated into ESMs. However, ESMs differ greatly in how they simulate terrestrial biological nitrogen fixation (BNF), the main natural nitrogen source to terrestrial ecosystems. We show that most ESMs inaccurately simulate terrestrial BNF, differing from a new global synthesis of terrestrial BNF measurements across natural and agricultural biomes. ESMs significantly underestimate agricultural BNF. ESMs overestimate BNF in forests and grasslands, which are the ecosystems with the greatest carbon uptake. As a result, ESMs could exaggerate plant carbon uptake as atmospheric CO_2 concentration rises.

The terrestrial biosphere currently sequesters approximately a quarter of anthropogenic CO_2 emissions (1). Terrestrial CO_2 sequestration has been enhanced by the CO_2 fertilization effect, in which rising atmospheric CO_2 concentration stimulates photosynthesis and plant growth (2). However, the CO_2 fertilization effect has declined globally over recent decades, indicating a weakening ability of the terrestrial biosphere to mitigate climate change (3). This recent global decline in the CO_2 fertilization effect is suggested to be driven, in part, by nutrient limitation of plant growth (3, 4). A nutrient of particular interest is nitrogen (N), an essential element for plant growth, which limits the productivity of the terrestrial biosphere and its capacity for CO_2 sequestration (5–7).

Anthropogenic activities such as fertilizer application in agriculture as well as fossil fuel combustion have substantially increased N loading in many regions of the terrestrial biosphere both directly as fertilizer and indirectly as atmospheric deposition (8). Simultaneously, N availability may be declining in many natural ecosystems due to rising atmospheric CO_2 concentration, suggested by decreasing N concentrations and isotope ratios in leaves, wood, and lake sediments alongside declining ecosystem N losses (9). Because natural ecosystems dominate the terrestrial CO_2 sink (10), global declines in N availability in natural ecosystems could compromise the persistence of the CO_2 fertilization effect (7).

Under N-poor conditions, plants employ various strategies to enhance N acquisition, overcome N limitation, and sustain growth. Plants can invest carbon (C) in fine root production (11) and mycorrhizal fungi (12) to enhance uptake of available soil N. Plants can also adjust their stoichiometry to increase C storage per unit N via higher tissue C:N ratios (13), or allocate more C to tissues with high C:N ratios such as wood (14). While these strategies influence how plants capitalize on existing N within an ecosystem, another strategy brings "new N" into ecosystems via biological nitrogen fixation (BNF): some plants can form symbiotic relationships with N-fixing bacteria, which transform

Author contributions: S.K.-G. designed research; S.K.-G. performed research; S.K.-G. wrote the initial draft of the paper; C.R.R.E., S.S.P., C.C.C., D.N.L.M., S.C.R., B.N.T., S.A.B., T.E.C., K.A.D., M.G., M.J.G., D.F.H., S.E.J., M.B.P., J.P., E.R.-C., V.G.S., F.M.S., A.P.S., B.W., C.A.W., and N.W. collected data; and C.R.R.E., S.S.P., C.C.C., D.N.L.M., S.C.R., B.N.T., S.A.B., T.E.C., K.A.D., M.G., M.J.G., D.F.H., S.E.J., M.B.P., J.P., E.R.-C., V.G.S., F.M.S., A.P.S., B.W., C.A.W., and N.W. edited the paper.

The authors declare no competing interest.

This article is a PNAS Direct Submission.

[1]To whom correspondence may be addressed. Email: sian_kou-giesbrecht@sfu.ca.

This article contains supporting information online at https://www.pnas.org/lookup/suppl/doi:10.1073/pnas.2514628122/-/DCSupplemental.

Published November 24, 2025.

Table 1. Description of BNF representations in ESMs

ESM	Land surface model	Symbiotic BNF: Natural BNF	Symbiotic BNF: Agricultural BNF	Free-living BNF
EC-Earth3-CC EC-Earth3-Veg	LPJ-GUESS	$BNF = 0.0102AET + 0.0524$ enters soil inorganic N pool		
MIROC-ES2L MIROC-ES2H	VISIT-e	$BNF = 0.5(0.0234AET + 0.0172)$ enters plant N pool	66% of root N uptake (N-fixing crop PFT) enters plant N pool	$BNF = 0.5(0.0234AET + 0.0172)$ enters litter N pool
CMCC-CM2-SR5 CMCC-ESM2 SAM0-UNICON TaiESM1	CLM4	$BNF = 1.8(1 - e^{-0.003NPP})$ enters soil inorganic N pool		
AWI-ESM-1-1-LR AWI-ESM-1-REcoM MPI-ESM1-2-HAM MPI-ESM1-2-LR MPI-ESM1-2-HR	JSBACH	$BNF = 1.8(1 - e^{-0.003NPP})$ enters soil inorganic N pool		
UKESM1-0-LL UKESM1-1-LL	JULES-ES	$BNF = 0.0016 \times NPP$ enters soil inorganic N pool		
CESM2 CESM2-FV2 CESM2-WACCM CESM2-WACCM-FV2 NorESM2-LM NorESM2-MM	CLM5	FUN model enters plant N pool	FUN model (N-fixing crop PFT) enters plant N pool	$BNF = (6.0AET + 0.702) \times 10^{-5}$ enters soil inorganic N pool

BNF is given in g N m^{-2} y^{-1}, AET is given in cm y^{-1}, and NPP is given in g C m^{-2} y^{-1}. PFT: plant functional type. See *SI Appendix*, Table S1 for more details.

atmospheric N_2 gas into a plant-available form of N (15). These plants can up-regulate BNF under N-limited conditions by allocating more C to their symbiotic N-fixing bacteria. Additionally, free-living forms of BNF, carried out by N-fixing microbes associated with mosses, lichens, biological soil crusts (biocrusts), litter, dead wood, and soil are important but often overlooked N sources (16). Overall, BNF has a high potential for enhancing N availability (15), yet the extent to which it can sustain elevated productivity under rising atmospheric CO_2 concentration is unclear.

Earth system models (ESMs) simulate and project the dynamics of the Earth system under global change, underlying the climate change projections in the Intergovernmental Panel on Climate Change (IPCC) reports (17). Incorporating N cycling into the land surface components of ESMs has been a focal point of recent ESM development, adopted by approximately half of ESMs in the most recent Coupled Model Intercomparison Project (CMIP6) for the IPCC Sixth Assessment Report (18). ESM simulations show a substantial CO_2 fertilization effect, but it is significantly lower in ESMs with terrestrial N cycling (which explicitly represent N limitation of plant growth) (18, 19). ESMs with terrestrial N cycling rely on varying assumptions and structures to represent key N cycling processes (20), and the impact of these assumptions on the modeled CO_2 fertilization effect is unclear. In particular, BNF has been identified as a key uncertainty in ESMs (21, 22). This is, in part because BNF is the dominant natural N flux to the terrestrial biosphere (15), and in part because the capacity for symbiotic BNF to respond to and alleviate N limitation is challenging to parse and to represent in silico but pivotal to the persistence of the CO_2 fertilization effect.

ESMs represent BNF in multiple ways (Table 1). Traditionally, ESMs have represented BNF phenomenologically as a function of net primary production (NPP) or actual evapotranspiration (AET), following conceptual and empirical evidence showing correlations between BNF rates and C supply, temperature, and water availability (15, 23). More recent efforts have represented BNF more mechanistically. For example, in the Fixation and Uptake of N (FUN) model, which is included in some ESMs (Table 1), plants optimize BNF to maximize their growth given both N limitation and the substantial C cost of BNF (24). FUN thus captures important underlying mechanisms such as the observed up-regulation of symbiotic BNF in N-limited conditions due to elevated atmospheric CO_2 concentration (25). Further, only a few ESMs distinguish between symbiotic BNF by agricultural crops (e.g., soybeans, alfalfa, etc.) versus natural vegetation. Similarly, only a few ESMs distinguish between symbiotic versus free-living BNF, despite significant differences in patterns and controls among these BNF niches (26). Studies focusing on a single model show that the representation of BNF has a significant impact on modeled terrestrial CO_2 sequestration (27, 28).

Because global BNF has been poorly constrained, with empirical estimates ranging from 40 to 290 Tg N y^{-1} (15, 21, 23), evaluating BNF in ESMs has been problematic, leaving the role of BNF in sustaining the CO_2 fertilization effect unclear. However, a recent global bottom–up synthesis of BNF observations substantially reduces the uncertainty of estimated global BNF, offering an opportunity to rigorously evaluate ESMs. This new synthesis incorporates over four times as many observations as prior syntheses and addresses the primary source of uncertainty in previous estimates by quantifying abundances of N-fixers across all major natural and agricultural N-fixing niches (26).

Here, we compare terrestrial BNF modeled in ESMs to observed terrestrial BNF from the new empirical BNF synthesis (26). We analyze 39 ESMs from CMIP6, 22 of which explicitly represent terrestrial N cycling. These 22 ESMs differ from each other in a number of ways, encompassing six different land surface models and five unique BNF representations (Table 1). We address the following questions: 1) How well do ESMs reproduce empirical estimates of present-day terrestrial BNF? 2) To what degree does enhanced BNF sustain the CO_2 fertilization effect in ESMs, and how does this compare to observations from elevated CO_2 experiments? 3) Is there a correlation between modeled BNF and the

CO_2 fertilization effect in ESMs and, if so, can observations of BNF be applied to this correlation to constrain the CO_2 fertilization effect?

Results and Discussion

Present-Day BNF. ESMs estimate that global terrestrial BNF is 111 Tg N y^{-1} with a range of 45 to 141 Tg N y^{-1} in the present-day (Fig. 1*A* and *SI Appendix*, Table S2). Observations from a new empirical BNF synthesis (26) estimate that global terrestrial BNF is 120 Tg N y^{-1} with a range of 106 to 136 Tg N y^{-1}. Despite the overlap of these global estimates, there are major discrepancies between ESMs and observations. The synthesis revealed that BNF in agricultural ecosystems (56 Tg N y^{-1}; 54 to 58 Tg N y^{-1}) is almost as high as BNF in natural ecosystems (65 Tg N y^{-1}; 52 to 77 Tg N y^{-1}). By contrast, ESMs suggest BNF within agricultural areas is only 10 Tg N y^{-1} in the present-day, which is ~46 Tg N y^{-1} lower than observations (Fig. 1*B*). Conversely, ESMs suggest BNF within natural areas is 100 Tg N y^{-1} in the present-day, exceeding observations by ~35 Tg N y^{-1} (Fig. 1*C*).

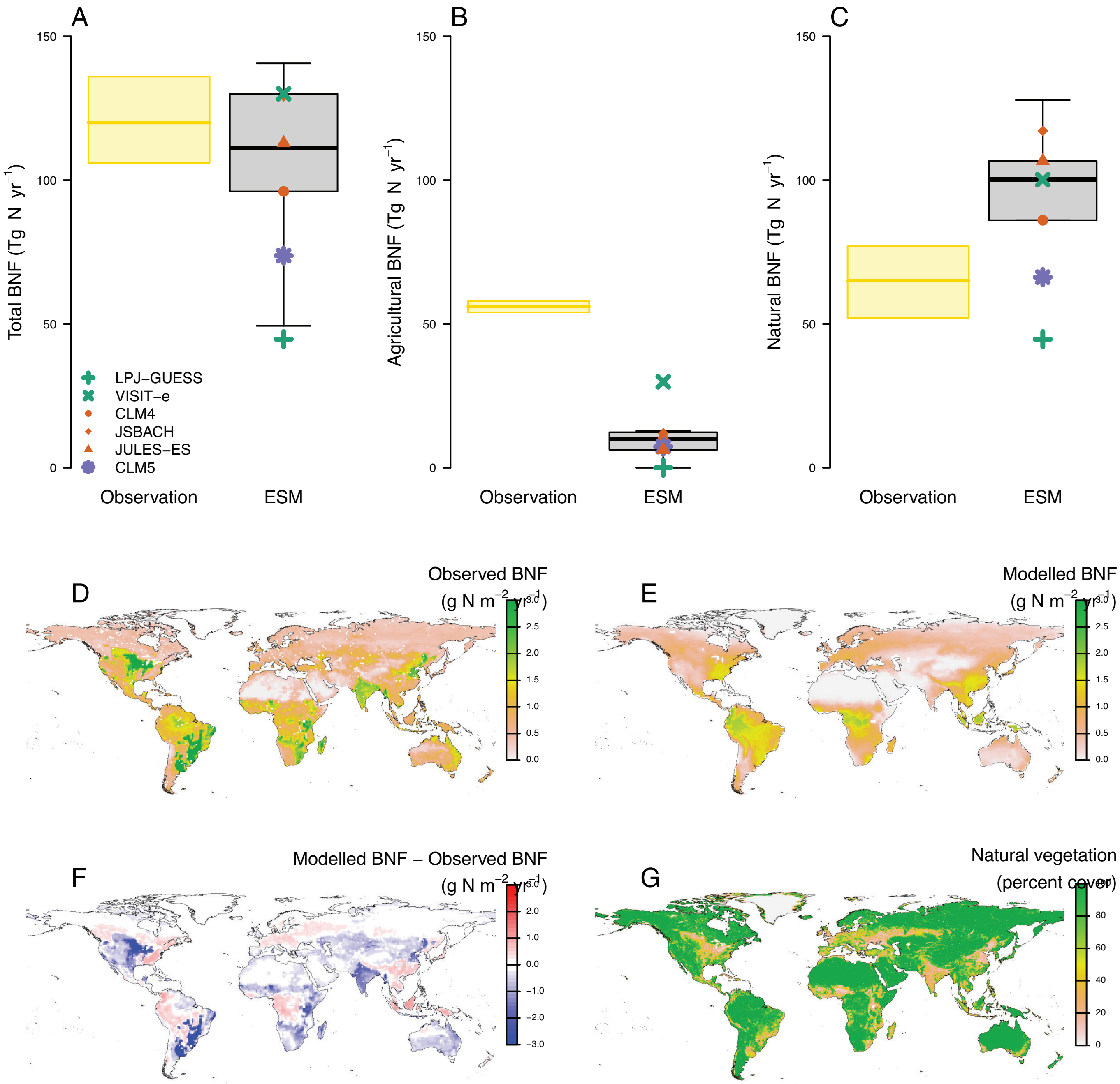

Fig. 1. Comparison between empirical and modeled present-day terrestrial BNF. (*A*) Total, (*B*) agricultural, and (*C*) natural global BNF from a new empirical BNF synthesis (26) and ESMs (averaged over 1995 to 2014). Gray boxplots indicate the median and interquartile range across ESMs, and whiskers indicate the minimum and maximum across ESMs. Each point represents the average of ESMs with the same land surface model. Different colors indicate different BNF representations (BNF_{AET} green; BNF_{NPP} orange; BNF_{FUN} purple). Values are given in *SI Appendix*, Table S2. (*D*) Map of empirical BNF. (*E*) Map of modeled BNF (median across ESMs, averaged over 1995 to 2014). (*F*) Discrepancy between empirical BNF and modeled BNF, where blue areas indicate underestimation by ESMs and red areas indicate overestimation by ESMs relative to observations. (*G*) Percent natural vegetation cover for each 1 degree grid cell (averaged over 1995 to 2014) from ref. 29. Maps of modeled BNF for individual ESMs are shown in *SI Appendix*, Fig. S1.

Crops exhibit high BNF rates (26), which leads to empirically observed hotspots of BNF in regions with a high proportion of agricultural area (Fig. 1*D*), such as central North America, eastern South America, eastern Africa, and eastern and southern Asia. In contrast, the highest modeled BNF rates occur primarily at low latitudes in tropical South America, Africa, and Asia (Fig. 1*E*). BNF representations in ESMs generally do not distinguish between natural and agricultural BNF (Table 1). As such, the greatest discrepancies between empirical and modeled BNF occur in agricultural areas (Fig. 1 *F* and *G* and *SI Appendix*, Fig. S2).

The majority of ESMs represent BNF as a function of NPP or AET, based on the links between BNF rates and C supply, temperature, and water availability (15, 23). Newer BNF representations employ a resource optimization framework—the FUN model (Table 1). ESMs with BNF representations based on AET, NPP, and FUN (hereafter, BNF_{AET}, BNF_{NPP}, and BNF_{FUN} representations, respectively) yield relatively similar global BNF estimates in the present-day despite different structural and parametric implementations of BNF (*SI Appendix*, Fig. S3). While ESMs simulate present-day AET and NPP reasonably well [yielding high-performance scores when compared to observations (30, 31)],

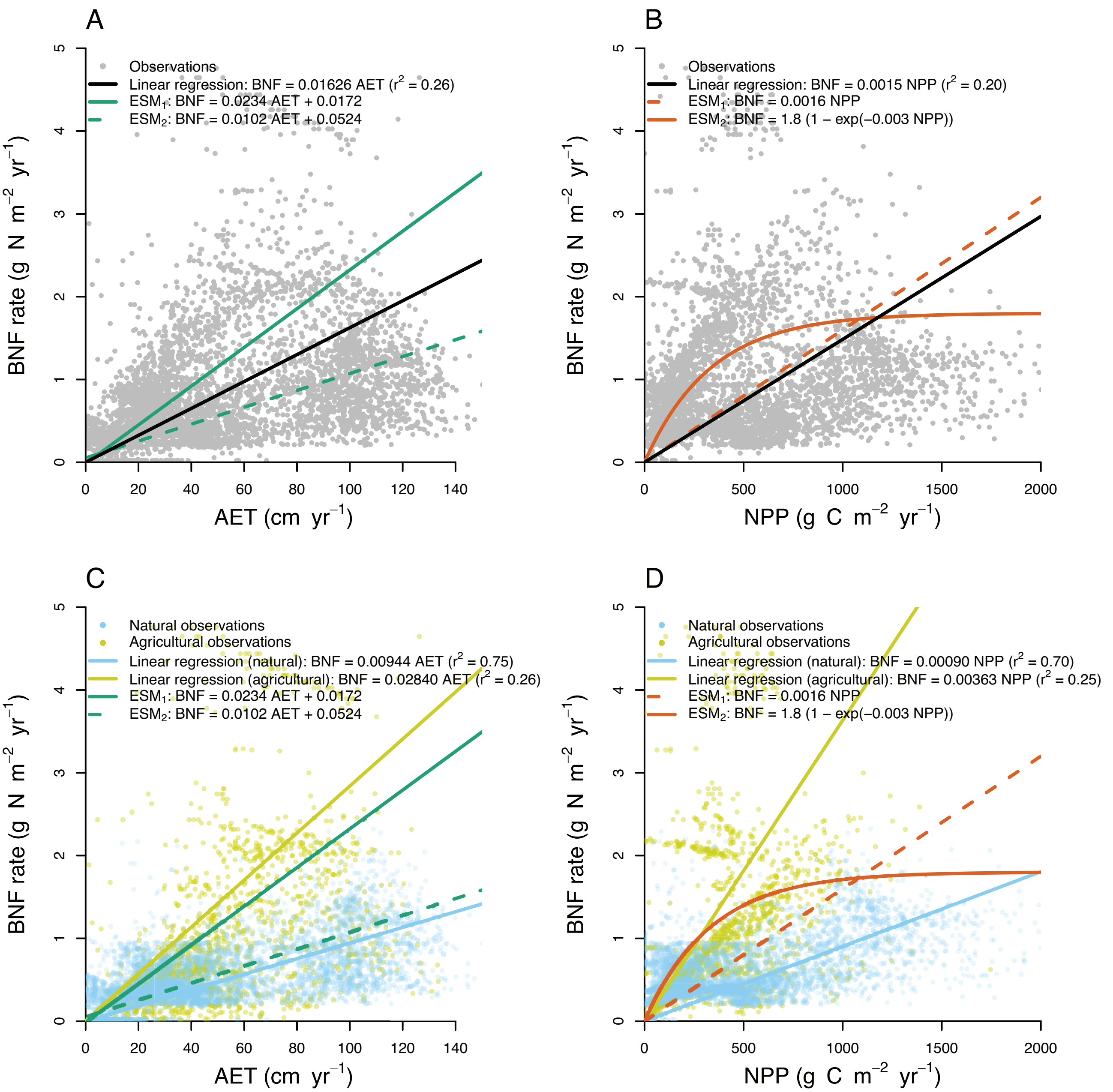

Fig. 2. Relationships between terrestrial BNF and AET and between terrestrial BNF and NPP that are implemented in ESMs compared to relationships derived from a new empirical BNF synthesis (26). (*A*) Total BNF (natural and agricultural) as a function of AET. (*B*) Total BNF (natural and agricultural) as a function of NPP. (*C*) Natural BNF and agricultural BNF as functions of AET. (*D*) Natural BNF and agricultural BNF as functions of NPP. BNF observations are from ref. 26 (a sample of 20,000 grid cell values at regular intervals), AET observations are from ref. 30, and NPP observations are from ref. 31. BNF representations in ESMs are described in Table 1 (note that ESMs employ multiple functions of both AET and NPP, indicated by the solid and dashed lines denoted as ESM_1 and ESM_2). We show linear regressions with the intercept forced through zero because zero AET or NPP should correspond to zero BNF when implemented in ESMs. Statistical metrics for linear regressions and linear regressions with nonzero intercepts are given in *SI Appendix*, Table S3.

they do a poor job of simulating present-day BNF [yielding a low-performance score when compared to the new empirical BNF synthesis (26)] (see *Materials and Methods* for a description of performance scores and *SI Appendix*, Figs. S4 and S5).

The new empirical BNF synthesis (26) yields different relationships between BNF and AET/NPP than those currently implemented in ESMs with BNF_{AET} and BNF_{NPP} representations (Fig. 2 *A* and *B* and *SI Appendix*, Table S3). Further, while most ESMs use the same representation for both natural and agricultural BNF (Table 1), the new empirical BNF synthesis yields BNF–AET and BNF–NPP relationships for natural ecosystems that give substantially lower BNF values for a given AET or NPP value than those for agricultural ecosystems (Fig. 2 *C* and *D*). Natural ecosystem relationships also have stronger explanatory power than those for agricultural ecosystems (higher r^2 and lower RMSE; *SI Appendix*, Table S3). The differing parameterizations for natural and agricultural BNF from the new empirical BNF synthesis (Fig. 2 *C* and *D*) are masked when natural and agricultural BNF are aggregated (Fig. 2 *A* and *B*) and lead to the underestimation of agricultural BNF and overestimation of natural BNF (Fig. 1). This could also be important for simulating N losses in ESMs, such as N_2O, NO_x, NH_3, and HONO emissions, N aerosol emissions, and N leaching, which are predominantly due to agriculture and have severe impacts on the climate system (32, 33) as well as aquatic eutrophication (34).

Within natural ecosystems, observations show that symbiotic BNF contributes 28 Tg N y^{-1} (25 to 31 Tg N y^{-1}) whereas free-living BNF contributes 36 Tg N y^{-1} (31 to 41 Tg N y^{-1}) (26), representing over half of total natural BNF (Fig. 3*A*). BNF representations in ESMs generally do not distinguish between symbiotic and free-living BNF (Table 1). ESMs overestimate BNF in forests, shrublands, savannas, and grasslands but underestimate BNF in barren areas in comparison to observations (Fig. 3*A*). This is likely because free-living BNF is a substantial contributor to BNF in barren areas. ESMs are thus overestimating BNF in the biomes contributing most to CO_2 sequestration, i.e., with the highest net ecosystem production (NEP) (Fig. 3 *B* and *C*). These empirical-modeled discrepancies in different regions are masked when examining the magnitude of global total BNF because the large discrepancies in agricultural versus natural BNF and between different biomes coincidentally cancel each other out, leading to equifinality of global total BNF but disguising underlying problems for simulating N supply and the terrestrial CO_2 sink.

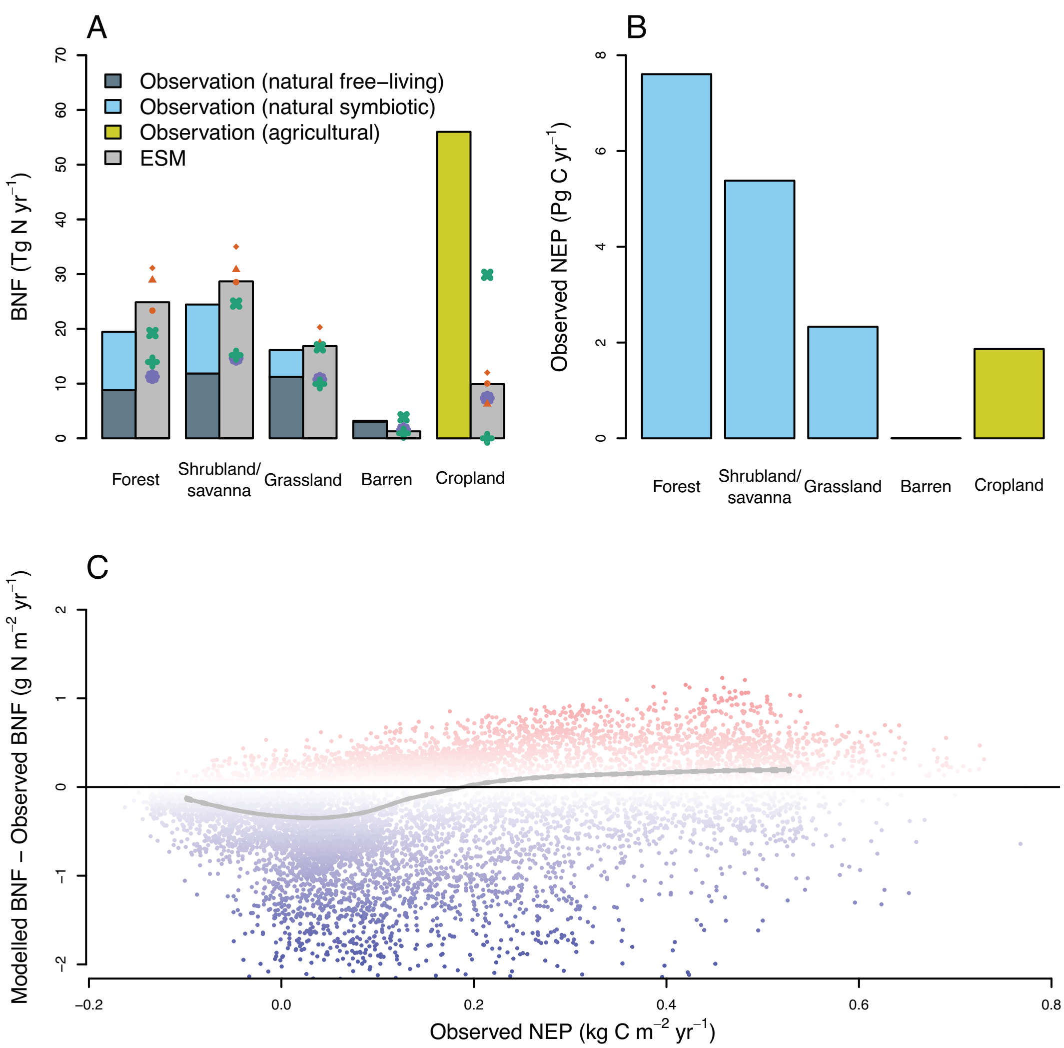

Fig. 3. Comparison between empirical and modeled present-day terrestrial BNF across biomes relative to NEP. (*A*) Empirical and modeled BNF (median and interquartile range) across International Geosphere–Biosphere Programme (IGBP) biomes (35), where empirical BNF is separated into free-living BNF and symbiotic BNF. Each point represents the average of ESMs with the same land surface model, and colors and shapes match Fig. 1. (*B*) Empirical NEP across IGBP biomes from ref. 36. (*C*) Discrepancy between empirical BNF and modeled BNF over NEP, where blue areas indicate underestimation by ESMs and red areas indicate overestimation by ESMs relative to observations. Each point is a grid cell.

Overall, ESMs are overestimating BNF in the most productive biomes—forests and grasslands—which are the largest contributors to the terrestrial CO_2 sink. Because BNF has a high potential to enhance N availability and sustain elevated productivity under rising atmospheric CO_2 concentration (21, 27, 28), this raises the possibility that ESMs are overestimating the CO_2 fertilization effect.

BNF and the CO_2 Fertilization Effect. Experimental ESM simulations in which atmospheric CO_2 concentration increases at 1% per year from its preindustrial value ("1pctCO2 experiments") are used to quantify the CO_2 fertilization effect (18). Here, we calculate the CO_2 fertilization effect as gross primary production (GPP) by natural ecosystems when atmospheric CO_2 concentration is twice the preindustrial level relative to GPP when atmospheric CO_2 concentration is at the preindustrial level, hereafter "GPP(2xCO_2)/GPP(1xCO_2)." In line with previous work (17, 18) and using a larger suite of 39 ESMs (*SI Appendix*, Table S4), we find that ESMs with terrestrial N cycling display a significantly lower CO_2 fertilization effect than ESMs without terrestrial N cycling ($P < 0.05$; Fig. 4*A*).

Within ESMs with terrestrial N cycling, CO_2 fertilization effects vary depending on how BNF is represented. ESMs with BNF_{AET} representations show modest CO_2 fertilization effects (24% increase with a doubling of CO_2; Fig. 4*A*), reflecting small increases in AET and thus small increases in natural BNF with rising atmospheric CO_2 concentration (6% increase with a doubling of CO_2; Fig. 4 *B* and *C*). In contrast, ESMs with BNF_{NPP} representations show higher CO_2 fertilization effects (47% increase with a doubling of CO_2), reflecting large increases in NPP and thus large increases in natural BNF with rising atmospheric CO_2 concentration (26% increase with a doubling of CO_2; Fig. 4 *B* and *C*). CLM4 is an exception, and analyses of CLM4 have identified overly strong N limitation that likely constrained the increase in NPP and thus natural BNF (37), which was remedied in CLM5 (which also shifted to a BNF_{FUN} representation). ESMs with mechanistic BNF_{FUN} representations show an intermediate CO_2 fertilization effect (38% increase with a doubling of CO_2) but a disproportionately large natural BNF increase (135% with a doubling of CO_2).

To benchmark the modeled BNF response to rising atmospheric CO_2 concentration, we conducted a meta-analysis of natural BNF in elevated CO_2 experiments and found a 31% (14 to 49%) natural BNF increase with a doubling of CO_2. The meta-analysis aligns with the 26% increase in ESMs with BNF_{NPP} representations and is higher than the 6% increase in ESMs with BNF_{AET} representations. However, the meta-analysis suggests a substantially lower response than the 135% increase in natural BNF in ESMs with BNF_{FUN} representations (Fig. 4*B*).

Our findings suggest that the choice of how to represent BNF underlies the simulated CO_2 fertilization effect in ESMs. While ESMs with different BNF representations yield relatively similar estimates of present-day BNF (Fig. 1), they yield starkly different estimates of BNF under rising atmospheric CO_2 concentration (Fig. 4*B*). ESMs with BNF_{AET} representations have a low CO_2 fertilization effect: AET increases marginally, causing BNF to increase marginally, implying strong sustained N limitation of CO_2 fertilization. AET increases marginally because water use efficiency is enhanced at higher CO_2 concentration (38, 39). This occurs in ESMs both with and without terrestrial N cycling (Fig. 4*C*) suggesting that AET drives BNF, which drives the CO_2

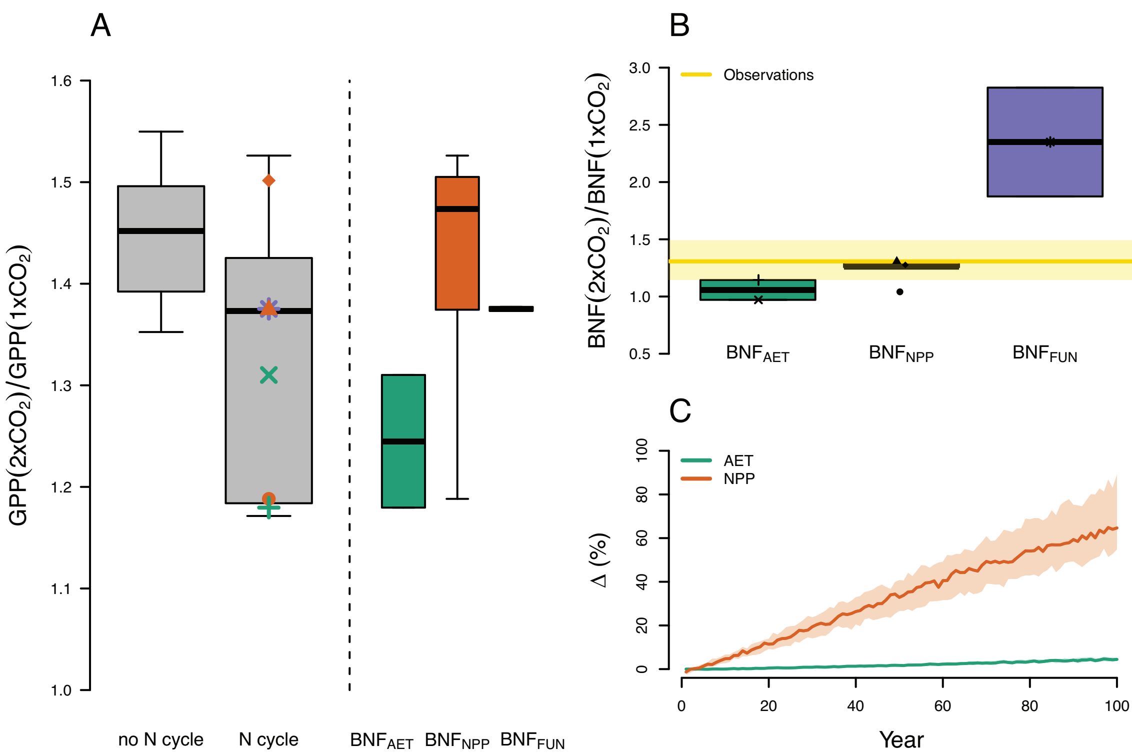

Fig. 4. CO_2 fertilization effect and natural terrestrial BNF under rising atmospheric CO_2 concentration simulated by ESMs. (*A*) CO_2 fertilization effect (GPP(2xCO_2)/GPP(1xCO_2)) for ESMs with and without terrestrial nitrogen (N) cycling. (*B*) Natural BNF when atmospheric CO_2 concentration is twice the preindustrial level relative to natural BNF when atmospheric CO_2 concentration is at the preindustrial level (BNF(2xCO_2)/BNF(1xCO_2)) for ESMs with different BNF representations compared to a meta-analysis of natural BNF in elevated CO_2 experiments. (*C*) Percent change in AET and NPP over 100 y of the 1pctCO2 experiments for all ESMs. Shading indicates the interquartile range. Boxplots indicate medians and the interquartile range, and whiskers indicate the minimum and maximum across ESMs. Each point represents the average of ESMs with the same land surface model, and colors and shapes match Fig. 1. Individual ESMs are shown in *SI Appendix*, Fig. S6, and latitudinal patterns are shown in *SI Appendix*, Fig. S7.

fertilization effect. This is also problematic because AET (and thus BNF) becomes decoupled from productivity and C supply, which are underlying controls of BNF. ESMs with BNF_{NPP} representations tend to have a higher CO_2 fertilization effect due to an amplifying feedback loop: NPP increases substantially as photosynthesis is enhanced at higher CO_2 concentration in ESMs (38, 39), causing BNF to increase substantially, alleviating N limitation of CO_2 fertilization, and further increasing NPP. ESMs that mechanistically incorporate the up-regulation of symbiotic BNF in N-limited conditions—BNF_{FUN} representations—exhibit an enormous increase in natural BNF, exceeding observations from elevated CO_2 experiments. Despite this, ESMs with BNF_{FUN} representations yield only a moderate CO_2 fertilization effect. This is likely because a significant fraction of increased productivity supported by up-regulated BNF is respired as a C cost of BNF, canceling out to a moderate CO_2 fertilization effect. On the other hand, BNF_{AET} and BNF_{NPP} representations do not account for the substantial C cost of BNF (24), which would detract from the CO_2 fertilization effect.

Overall, all BNF representations in ESMs fall short of fully capturing BNF-C interactions under rising atmospheric CO_2 concentration. ESMs with BNF_{AET} representations simulate an unrealistically low BNF response and thus low CO_2 fertilization effect. ESMs with BNF_{NPP} representations simulate a reasonable BNF response but neglect the substantial C cost of BNF and thus likely overestimate the CO_2 fertilization effect over time. ESMs with BNF_{FUN} representations simulate an unrealistically high BNF response but more realistically account for both the C cost of BNF and its regulation by N limitation.

Next Steps for Improving the Representation of BNF in ESMs. Based on both our model-observation comparison of global terrestrial BNF in the present day and its response to rising atmospheric CO_2 concentration, we outline a series of suggestions for modeling terrestrial BNF in ESMs.

First, we suggest simulating agricultural and natural BNF separately in ESMs (Figs. 1 and 2). Observations show that agricultural ecosystems exhibit significantly higher BNF rates than natural ecosystems, largely because the dominant controls differ. While agricultural BNF is driven primarily by cropland and/or pasture composition as well as management strategies that favor high BNF rates (40), natural BNF is more strongly regulated by physiological and community-level processes (15). Agriculture strongly influences the global distribution of BNF. Distinguishing between agricultural and natural BNF in models is important for simulating the CO_2 fertilization effect and its spatial pattern with ESMs, given that natural ecosystems drive the terrestrial CO_2 sink, but natural BNF is overestimated in ESMs. It is also extremely important for accurately simulating N losses and their spatial pattern. However, agricultural BNF is only explicitly distinguished in one out of five land surface models in ESMs (Table 1).

Second, we suggest simulating symbiotic and free-living BNF separately in ESMs (Fig. 3). This would be an important step forward because symbiotic and free-living BNF rates have different optimal conditions and controls (16, 41), such as differing temperature optima (42). Additionally, symbiotic and free-living BNF supply different ecosystem N pools: Symbiotic BNF directly contributes to plant N uptake and sustains plant productivity, whereas free-living BNF enters the litter or soil N pools (among other niches). Free-living BNF contributes over half of total natural BNF but is only distinguished in two out of five land surface models in ESMs (Table 1).

We contextualize these two suggestions with simple back of the envelope calculations. ESMs suggest global natural BNF is 100 $Tg\ N\ y^{-1}$ in the present-day, which exceeds observations (65 $Tg\ N\ y^{-1}$) by ~35 $Tg\ N\ y^{-1}$. This implies that natural ecosystems are receiving ~35 $Tg\ N\ y^{-1}$ from an unaccounted N source in ESMs. Assuming that this BNF supports CO_2 sequestration and a plant C:N ratio of 100:1 (43), this N surplus supports sequestration of ~3.5 $Pg\ C\ y^{-1}$ which is ~7% of present-day natural NPP [50 $Pg\ C\ y^{-1}$ (31)]. If we only consider symbiotic BNF (29 $Tg\ N\ y^{-1}$) and exclude free-living BNF (36 $Tg\ N\ y^{-1}$), aligning modeled and observed global natural BNF brings the total overestimation of global natural BNF by ESMs to ~71 $Tg\ N\ y^{-1}$. This N surplus supports sequestration of ~7.1 $Pg\ C\ y^{-1}$, i.e., ~14% of present-day natural NPP is supported by an unaccounted N source in ESMs. This discrepancy would amplify as BNF increases under rising atmospheric CO_2 concentration. While there are several caveats associated with these extrapolations, they contextualize the importance of modeling natural vs. agricultural and symbiotic vs. free-living BNF for both the terrestrial C sink and agricultural N gas emissions in ESMs.

Third, we argue that a new representation of symbiotic BNF in ESMs is warranted given the limitations of each existing representation in capturing the response of BNF to rising atmospheric CO_2 concentration (Fig. 4). Because most ESMs use a phenomenological BNF representation and because overhauling process representations in ESMs is challenging, it is likely that many ESMs will continue to use a phenomenological BNF representation for some time. For these ESMs, we recommend using a BNF_{NPP} representation over a BNF_{AET} representation. While AET integrates two important controls on both BNF and productivity—temperature and water availability—its relationship to C supply becomes decoupled under rising atmospheric CO_2 concentration. Thus, we argue it is more appropriate to use NPP over AET as a driver to simulate BNF. We provide updated relationships between BNF and NPP in Fig. 2 (and *SI Appendix*, Fig. S8 which focuses on symbiotic BNF), which are a simple shift that could be readily implemented in ESMs. Importantly, this new symbiotic BNF representation should build on the original BNF_{NPP} representation by also incorporating the C cost of BNF. Independently, we believe it is essential to advance mechanistic BNF representations that can capture the regulation of symbiotic BNF by N limitation such as in the BNF_{FUN} representation (25), other ecosystem models (44, 45), and newer terrestrial biosphere models (27, 46). The regulation of symbiotic BNF by N limitation not only underlies the response of BNF to rising atmospheric CO_2 concentration but also is important for capturing its response to changing atmospheric N deposition (47). Higher atmospheric N deposition could alleviate N limitation of CO_2 fertilization to some extent (48). However, updated symbiotic BNF representations should incorporate physiological limitations to BNF to prevent "runaway" BNF. Mechanistic BNF representations should be advanced to ensure that they are ready for adoption when ESMs currently using phenomenological BNF representations are prepared to transition to such a more complex and comprehensive approach.

Finally, as more ESMs incorporate other plant strategies that alleviate N limitation (e.g., flexible tissue allocation, stoichiometry, and mycorrhizae), these should be considered in parallel to symbiotic BNF (*SI Appendix*, *Supplementary Text*). As more ESMs incorporate terrestrial phosphorus (P) cycling, interactions between C, N, and P cycles should also be considered. P regulates symbiotic BNF, both because BNF requires P-rich metabolites and because it promotes plant growth which in turn increases P demand (49, 50). Novel representations of symbiotic BNF in ESMs can and should be evaluated through comparison to observations from experimental manipulations such as CO_2 enrichment experiments as well as concurrent warming or N and P fertilization experiments. Benchmarking models against such experiments allows for the identification of model limitations in simulating appropriate ecosystem responses to future environmental change and their consequences (37).

BNF Constrains the CO_2 Fertilization Effect in ESMs. Emergent constraints have gained prominence as a method to reduce uncertainty in future projections by ESMs (51, 52). The concept is that, despite a large spread across ESMs, there are strong statistical relationships between simulated aspects of the current Earth system and simulated aspects of the future Earth system that only "emerge" when examining a suite of ESMs, transcending differences in structures and parameterizations across ESMs. Given these emergent relationships, observations of the current Earth system can be used to generate a "constraint" on ESM projections. BNF has a robust basis as an emergent constraint on the CO_2 fertilization effect as the dominant natural N source to the terrestrial biosphere needed to support new plant growth and CO_2 sequestration, as demonstrated by our analysis of its role in regulating the CO_2 fertilization effect above.

We find a positive correlation between modeled present-day natural BNF and the modeled CO_2 fertilization effect across ESMs with BNF_{NPP} and BNF_{AET} representations ($P < 0.05$; ESMs with BNF_{FUN} were not included because they do not capture the observed response of BNF to elevated CO_2). Using the framework of emergent constraints, we apply the new empirical BNF synthesis (26) to the emergent relationship between present-day natural BNF and the CO_2 fertilization effect (Fig. 5*A*). After the observational constraint is applied, the CO_2 fertilization effect is reduced from 1.33 (1.20 to 1.46) in the equal-weighted mean for ESMs with terrestrial N cycling to 1.23 (1.10 to 1.33), i.e., by 8% (Fig. 5*B*). Applying the observational constraint to the equal-weighted mean for ESMs without terrestrial N cycling, which is 1.45 (1.38 to 1.51), reduces the CO_2 fertilization effect by 15%. Applying the observational constraint to the equal-weighted mean for all ESMs, which is 1.38 (1.26 to 1.50), reduces the CO_2 fertilization effect by 11%.

Conclusions. Overall, while ESMs reproduce the empirically observed magnitude of global total terrestrial BNF (26), they greatly underestimate agricultural BNF and overestimate natural BNF in the most productive biomes that are the largest contributors to the terrestrial CO_2 sink. Our findings suggest that the way BNF is represented strongly influences the CO_2 fertilization effect in ESMs and that current BNF representations in ESMs fall short of fully capturing both its present-day patterns and its response to rising atmospheric CO_2 concentration. Moving forward, we offer a number of strategies for revising and improving the representation of BNF in ESMs, highlighting the importance of implementing key processes such as agricultural BNF, free-living BNF, the C cost of BNF, and its response to N limitation. Finally, we constrain the simulated CO_2 fertilization effect with a new empirical BNF synthesis. We show that, due to their overestimation of natural BNF, ESMs, especially those without terrestrial N cycling, are likely exaggerating the CO_2 fertilization effect and the capacity of the terrestrial CO_2 sink to mitigate climate change.

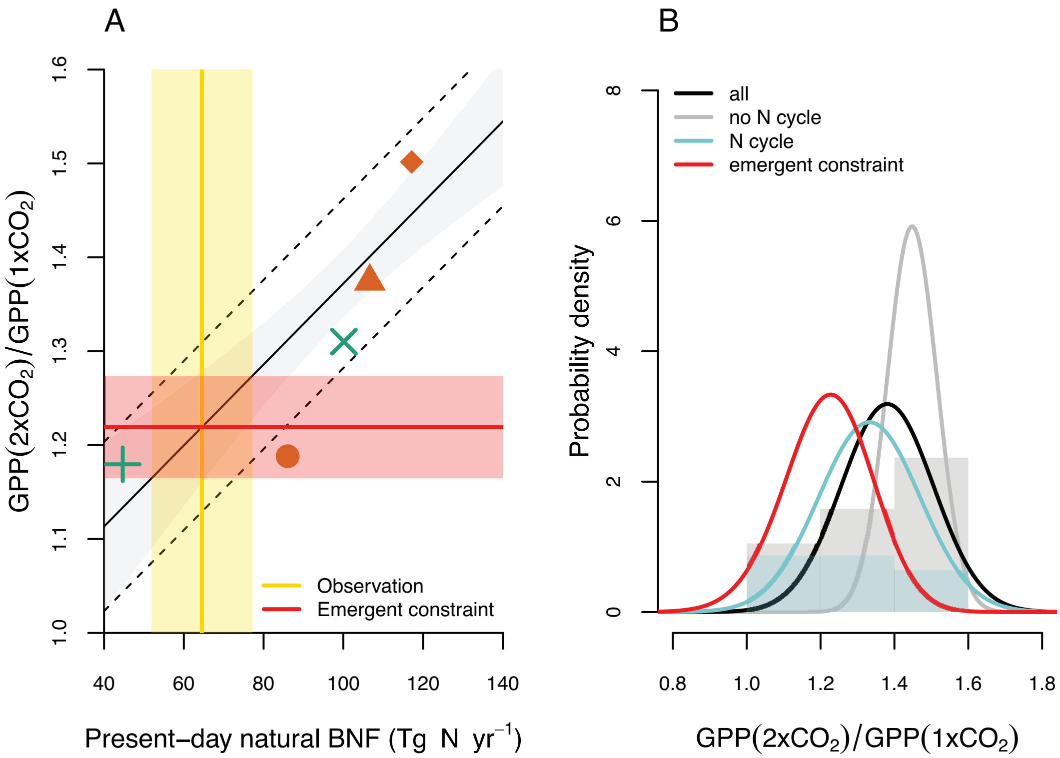

Fig. 5. Relationship and emergent constraint of natural terrestrial BNF on the CO_2 fertilization effect. (*A*) Relationship between modeled present-day natural BNF and the CO_2 fertilization effect ($GPP(2xCO_2)/GPP(1xCO_2)$). Each point represents the average of ESMs with the same land surface model, and colors and shapes match Fig. 1. Individual ESMs are shown in *SI Appendix*, Fig. S9. The solid black line is a linear regression. The gray shaded region shows the 66% CI of the linear regression. The dashed black lines show the residual SE. Observations (26) are indicated by the vertical yellow line and yellow shaded region. The horizontal red line, which shows the intersection of the range of observations and the linear regression, indicates the emergent constraint of BNF on the CO_2 fertilization effect. (*B*) Probability density functions of $GPP(2xCO_2)/GPP(1xCO_2)$. The gray histogram shows the distribution of all ESMs, and the black line is a Gaussian distribution with the same mean and SD. The gray line is the Gaussian distribution corresponding to ESMs without terrestrial N cycling. The blue histogram shows the distribution of ESMs with terrestrial N cycling, and the blue line is a Gaussian distribution with the same mean and SD. The red line shows the emergent constraint. Values are given in *SI Appendix*, Table S5.

Materials and Methods

Global BNF Observations. We used a new bottom–up empirical synthesis of global terrestrial BNF that upscales field measurements using abundances of natural N-fixing niches (trees, shrubs, herbs, ground mosses, epiphytic lichens, biocrusts, litter, dead wood, and soil) and agricultural N-fixing niches (legume crops and forage, rice, and sugarcane). It includes 1,177 published natural BNF rates and 5,473 published agricultural BNF rates along with corresponding abundance and distribution datasets to construct a global gridded product of present-day BNF at 0.004-degree resolution. Full details are given in refs. 26, 53, and 54.

To understand the relationships between observed BNF, AET, and NPP, we used linear regressions. We used the AET global gridded product at 0.04-degree resolution (average of 2000 to 2020) from TerraClimate (30). We used the NPP global gridded product at 0.004-degree resolution (average of 2001 to 2020) from MODIS/Terra (31). When conducting linear regressions, we used a sample of 20,000 grid cell values at regular intervals following ref. 26.

To analyze the observed response of natural BNF to rising atmospheric CO_2 concentration, we conducted a meta-analysis of BNF in elevated CO_2 experiments. We conducted a comprehensive literature search with the terms ("elevated CO_2" or "elevated carbon dioxide") and ("N fixation" or "N_2 fixation") using Google Scholar. Selected studies gave BNF rate in both a control and elevated CO_2 treatment and the CO_2 concentration in both treatments. We combined this list of studies with two previous meta-analyses (55) and (47). Liang et al. (55) used the search terms ("CO_2 enrichment" or "CO_2 increase"), ("nitrogen"), and ("terrestrial"). Zheng et al. (47) used the search terms ("carbon dioxide" or "CO_2") and ("nitrogen fixation" or N fixation or N_2 fixation or "dinitrogen fixation" or "nitrogenase"). Studies in refs. 47 and 55 were reexamined for CO_2 concentration in both treatments. The meta-analysis included free air CO_2 enrichment (FACE), growth chamber, and open top chamber experiments. It included acetylene reduction assay, ^{15}N isotope, and mass balance methods for measuring BNF. We only examined data points from natural ecosystems (forests and grasslands) that received no other treatments (e.g., no nutrient fertilization, drying, wetting, warming, cooling, etc.) for comparison to ESMs (which primarily do not represent agricultural BNF, Table 1). Both free-living and symbiotic BNF were included. We recorded mean, variation (SD or SE), and sample size (n) of the BNF rate in the control and elevated CO_2 treatments. Different species within the same study were recorded separately. If more than one value was provided during the experimental period, all values were averaged. If SE was provided, SD was calculated as $\mathrm{SD} = \mathrm{SE}\sqrt{n}$. If neither SD nor SE were provided, SD was assumed to be 25% of the mean. We also recorded CO_2 concentration in the control and elevated CO_2 treatments. If CO_2 concentration in the control treatment was not given ("ambient CO_2 concentration"), CO_2 concentration was extracted from NOAA Global Monitoring Laboratory (56) for the experimental period. Overall, 52 observations were included in the meta-analysis (15 of which were new, i.e., not included in either refs. 47 and 55).

We calculated the effect size of elevated CO_2 as the natural logarithm transformed response ratio ($\ln(\mathrm{RR})_i$) for each study i (57):

$$\ln(\mathrm{RR})_i = \ln\left(\frac{\mathrm{BNF}_{\mathrm{elevated},i}}{\mathrm{BNF}_{\mathrm{control},i}}\right). \qquad [1]$$

$\mathrm{BNF}_{\mathrm{elevated},i}$ is the mean BNF rate in the elevated CO_2 treatment of study i, and $\mathrm{BNF}_{\mathrm{control}}$ is the mean BNF rate in the control treatment of study i. The variance of $\ln(\mathrm{RR})_i$ (v_i) is

$$v_i = \frac{\mathrm{SD}^2_{\mathrm{control},i}}{n_{\mathrm{control},i}\mathrm{BNF}^2_{\mathrm{control},i}} + \frac{\mathrm{SD}^2_{\mathrm{elevated},i}}{n_{\mathrm{elevated},i}\mathrm{BNF}^2_{\mathrm{elevated},i}}. \qquad [2]$$

$\mathrm{SD}_{\mathrm{elevated},i}$ is the SD of the BNF rate in the elevated CO_2 treatment of study i, $\mathrm{SD}_{\mathrm{control},i}$ is the SD of the BNF rate in the control treatment of study i, $n_{\mathrm{elevated},i}$ is the sample size of the elevated treatment of study i, and $n_{\mathrm{control},i}$ is the sample size of the control treatment of study i.

We used a multilevel mixed-effects metaregression model in which the magnitude of CO_2 enrichment is a fixed effect and study is a random effect:

$$ln(\mathrm{RR})_i = \beta_0 + \beta_1\left(\left[\mathrm{CO}_{2,\mathrm{elevated},i}\right] - \left[\mathrm{CO}_{2,\mathrm{control},i}\right]\right) + \mu_{\mathrm{study},i} + \varepsilon_i. \qquad [3]$$

β_0 and β_1 are coefficients, $[\mathrm{CO}_{2,\mathrm{elevated},i}]$ is the CO_2 concentration in the elevated CO_2 treatment of study i, $[\mathrm{CO}_{2,\mathrm{control},i}]$ is the CO_2 concentration in the control treatment of study i, $\mu_{\mathrm{study},i}$ is the random effect, and ε_i is the sampling error. The weighted average and 95% CI of $\ln(\mathrm{RR})_i$ for a given magnitude of CO_2 enrichment were calculated using the standard inverse-variance method and restricted maximum likelihood estimation using the R package "metafor" (58).

There were no significant differences between different facilities or methods (*SI Appendix*, Table S6). Data collected for the meta-analysis are given as Dataset S1.

ESM Simulations. We used ESM outputs from the CMIP6 for historical simulations (1850 to 2014), which use prescribed atmospheric CO_2, and "1pctCO2 experiment" simulations (0 to 100 y), in which atmospheric CO_2 concentration increases at 1% per year from its preindustrial value. ESM outputs were downloaded from the Earth System Grid Federation (ESGF; https://aims2.llnl.gov/search/cmip6/): GPP (CMIP variable: gpp) and BNF (CMIP variable: fBNF). Percent crop cover (CMIP variable: cropFrac) was used to distinguish between natural and agricultural BNF (see below). Grid-cell area (CMIP variable: areacella) and land area fraction (CMIP variable: sftlf) were also used to calculate global totals.

We used all ESMs that provided the required outputs. 35 ESMs provided GPP output in 1pctCO2 experiment simulations (*SI Appendix*, Table S3). 11 ESMs provided GPP and BNF output in 1pctCO2 experiment simulations as well as BNF output in historical simulations (*SI Appendix*, Table S4). These ESMs are described in Table 1 and *SI Appendix*, Table S1. Overall, they span six different land surface models (LPJ-GUESS, VISIT-e, CLM4/4.5, JSBACH, JULES-ES, and CLM5) and five unique BNF representations. Different versions of the same ESM from the same institution were averaged. No ESMs included terrestrial P cycling.

To distinguish between agricultural and natural BNF, we assumed that grid cells with ≥40% crop cover were agricultural and grid cells with <40% crop cover were natural following ref. 26, where 40% is the minimum crop cover for a grid cell to be considered a cropland class in the IGBP system. This yielded an average total crop area of ~1,075 Mha between 1995 and 2014 across ESMs, which is comparable to 1,244 Mha from ref. 59. To distinguish BNF in each IGBP biome (35), we applied a mask where each grid cell was assigned to a different IGBP biome using the product at 0.004-degree resolution remapped to 1-degree resolution using nearest neighbor interpolation. Similarly, to distinguish NEP in each IGBP biome, we used the NEP global gridded product at 0.0833-degree resolution (average of 2001 to 2015) from FLUXCOM (36) remapped to 1-degree resolution using bilinear interpolation, and we applied a mask where each grid cell was assigned to a different IGBP biome.

To quantify the CO_2 fertilization effect, we calculated total GPP by natural ecosystems when atmospheric CO_2 concentration is twice the preindustrial level relative to total natural GPP when atmospheric CO_2 concentration is at the preindustrial level, hereafter $\mathrm{GPP(2xCO_2)/GPP(1xCO_2)}$ following ref. 60. We focused on natural ecosystems because of their contribution to the CO_2 fertilization effect and because agricultural N cycling is inconsistently represented by ESMs. We calculated $\mathrm{GPP(2xCO_2)/GPP(1xCO_2)}$ as the average GPP between Years 68 and 72 of the simulation (average atmospheric CO_2 concentration is 565 ppm) divided by the average GPP between years 8 and 12 of the simulation (average atmospheric CO_2 concentration is 284 ppm). We conducted the same calculation with BNF to calculate $\mathrm{BNF(2xCO_2)/BNF(1xCO_2)}$ as the average BNF between Years 68 and 72 of the simulation divided by the average BNF between years 8 and 12 of the simulation. Each ESM yields a single global value for $\mathrm{GPP(2xCO_2)/GPP(1xCO_2)}$ and $\mathrm{BNF(2xCO_2)/BNF(1xCO_2)}$. $\mathrm{BNF(2xCO_2)/BNF(1xCO_2)}$ was compared to the exponential of the weighted average and 95% CI of $\mathrm{lnln(RR)}_i$ for a magnitude of CO_2 enrichment of 284 ppm. However, we note that there are caveats to this comparison because CO_2 enrichment experiments used a step change in atmospheric CO_2 concentration for a short experimental period whereas, in the 1pctCO2 experiment simulations, atmospheric CO_2 concentration increases gradually.

ESM Performance. ESM performance in simulating BNF, AET, and NPP was calculated using two scores that assess the model's bias and spatial distribution relative to observations following ref. 61. Scores are dimensionless and range from 0 to 1, where a higher score value indicates better ESM performance. Equations for the scores are given in *SI Appendix*, *Supplementary Text*. Model outputs were compared to the new empirical BNF synthesis remapped to 1-degree resolution using bilinear interpolation and the NPP global gridded product at 0.004-degree resolution (average of 2001 to 2020) from MODIS/Terra remapped to 1-degree resolution using bilinear interpolation.

Emergent Constraint. The emergent constraint approach is used to achieve uncertainty reduction in the projected CO_2 fertilization effect (GPP(2xCO_2)/GPP(1xCO_2)) using the new empirical BNF synthesis and follows that of ref. 62. Despite a spread in both the CO_2 fertilization (y) and global total natural BNF (x) across ESMs, a relationship f emerges linking them: $y = f(x)$. The new empirical BNF synthesis, i.e., a measurement of x and its uncertainty, is used to constrain y. The following equations enable the calculation of the probability density of y ($P(y)$):

$$P(y) = \int_{-\infty}^{\infty} P(y|x)P(x)dx. \quad [4]$$

$P(x)$ is the probability density of x, which is assumed to have a Gaussian distribution:

$$P(x) = \frac{1}{\sqrt{2\pi\sigma_{obs}^2}} e^{-\frac{1}{2}\left(\frac{x-\mu_{obs}}{\sigma_{obs}}\right)^2}. \quad [5]$$

μ_{obs} is the mean of the new empirical BNF synthesis and σ_{obs} is the SD of the new empirical BNF synthesis (26). $P(y|x)$ is the probability density of the CO_2 fertilization effect given global total natural BNF and is assumed to have a Gaussian distribution:

$$P(y|x) = \frac{1}{\sqrt{2\pi\left(\sigma_f(x)\right)^2}} e^{-\frac{1}{2}\left(\frac{y-f(x)}{\sigma_f(x)}\right)^2}. \quad [6]$$

$f(x)$ is the linear regression (ordinary-least-squares method) between the modeled global total natural BNF and CO_2 fertilization effect. $\sigma_f(x)$ is the x-dependent prediction error of this linear regression:

$$\sigma_f(x) = s\sqrt{1 + \frac{1}{N} + \frac{(x-\bar{x})^2}{\sum_{i=1}^{N}(x_i-\bar{x})^2}}. \quad [7]$$

s is the SE of the linear regression, N is the number of ESMs, and $\bar{x}$ is the average of modeled global total natural BNF.

All analyses were performed in R (63) and used the package "terra" (64).

Data, Materials, and Software Availability. Dataset data have been deposited in meta-analysis of BNF in elevated CO_2 experiments (https://doi.org/10.5281/zenodo.15612191). Previously published data were used for this work (53, 54).

ACKNOWLEDGMENTS. This paper is a contribution from a working group on biological nitrogen fixation supported by the U.S. Geological Survey (USGS) John Wesley Powell Center for Analysis and Synthesis. S.K.-G. was supported by the Natural Sciences and Engineering Research Council of Canada's Discovery Grant Program (RGPIN-2024-04188). V.G.S. is supported by United States Department of Energy Office of Science Biological and Environmental Research to UT-Battelle, LLC grant DE-AC05-00OR22725 and the NGEE-Arctic project. The views and conclusions in this article represent those of USGS and represent those solely of the authors from Oak Ridge Associated Universities/Oak Ridge Institute for Science and Education and the U.S. Forest Service. Any use of trade, firm, or product names is for descriptive purposes only and does not imply endorsement by the U.S. Government. We thank Paige MacCarthy for her assistance with the meta-analysis. We thank Lauren Gover and Renée Hall for their feedback on the manuscript.

Author affiliations: [a]School of Resource and Environmental Management, Simon Fraser University, Burnaby, BC V5A 1S6, Canada; [b]Oak Ridge Institute for Science and Education, Oak Ridge, TN 37830; [c]United States Geological Survey, Forest and Rangeland Ecosystem Science Center, Corvallis, OR 97331; [d]Department of Ecosystem and Conservation Sciences, W.A. Franke College of Forestry and Conservation, University of Montana, Missoula, MT 59812; [e]Department of Ecology, Evolution, and Environmental Biology, Columbia University, New York, NY 10027; [f]United States Geological Survey, Southwest Biological Science Center, Moab, UT 84532; [g]Department of Organismic and Evolutionary Biology, Harvard University, Roslindale, MA 02131; [h]Cary Institute of Ecosystem Studies, Millbrook, NY 12545; [i]School of Geography, University of Leeds, Leeds LS2 9JT, United Kingdom; [j]Smithsonian Tropical Research Institute, Ancon 0843-03092, Panama; [k]The Land Institute, Salina, KS 67401; [l]Association for Tropical Biology and Conservation, Minneapolis, MN 55406; [m]Department of Forest Ecology and Management, Swedish University of Agricultural Sciences, Umea 90183, Sweden; [n]School of Environmental and Rural Science, University of New England, Armidale, NSW 2351, Australia; [o]United States Department of Agriculture Forest Service Pacific Northwest Research Station, Portland, OR 97204; [p]Commonwealth Scientific and Industrial Research Organisation Agriculture and Food, Canberra, ACT 2601, Australia; [q]Department of Built Environment, Aalto University, Espoo 00076, Finland; [r]Centro de Investigación de Colecciones Científicas de la Universidad de Almería y Departamento de Agronomía, Universidad de Almería, Almería 04120, Spain; [s]Multiphase Chemistry Department, Max Planck Institute for Chemistry, Mainz 55128, Germany; [t]Environmental Science Division, Oak Ridge National Laboratory, Oak Ridge, TN 37831; [u]Department of Biology and School of the Environment, McGill University, Montreal, QC H3A 1B1, Canada; [v]Earthshot Labs, Mill Valley, CA 94941; [w]Division of Plant Sciences, Institute for Biology, University of Graz, Graz 8010, Austria; [x]Graduate School of Geography, Clark University, Worcester, MA 01610; and [y]Odum School of Ecology, University of Georgia, Athens, GA 30602

1. P. Friedlingstein *et al.*, Global carbon budget 2024. *Earth Syst. Sci. Data* **17**, 965–1039 (2025).
2. S. Ruehr *et al.*, Evidence and attribution of the enhanced land carbon sink. *Nat. Rev. Earth Environ.* **4**, 518–534 (2023), 10.1038/s43017-023-00456-3.
3. S. Wang *et al.*, Recent global decline of CO_2 fertilization effects on vegetation photosynthesis. *Science* **370**, 1295–1300 (2020).
4. W. K. Smith *et al.*, Large divergence of satellite and Earth system model estimates of global terrestrial CO_2 fertilization. *Nat. Clim. Change* **6**, 306–310 (2016).
5. D. S. LeBauer, K. K. Treseder, Nitrogen limitation of net primary productivity in terrestrial ecosystems is globally distributed. *Ecology* **89**, 371–379 (2008).
6. E. Du *et al.*, Global patterns of terrestrial nitrogen and phosphorus limitation. *Nat. Geosci.* **13**, 221–226 (2020).
7. C. Terrer *et al.*, Nitrogen and phosphorus constrain the CO_2 fertilization of global plant biomass. *Nat. Clim. Change* **9**, 684–689 (2019).
8. D. Fowler *et al.*, The global nitrogen cycle in the twenty-first century. *Philos. Trans. R. Soc. Lond. B Biol. Sci.* **368**, 20130164 (2013).
9. R. E. Mason *et al.*, Evidence, causes, and consequences of declining nitrogen availability in terrestrial ecosystems. *Science* **376**, eabh3767 (2022).
10. F. Krausmann *et al.*, Global human appropriation of net primary production doubled in the 20th century. *Proc. Natl. Acad. Sci. U.S.A.* **110**, 10324–10329 (2013).
11. H. Poorter *et al.*, Biomass allocation to leaves, stems and roots: Meta-analyses of interspecific variation and environmental control. *New Phytol.* **193**, 30–50 (2012).
12. C. Averill, J. M. Bhatnagar, M. C. Dietze, W. D. Pearse, S. N. Kivlin, Global imprint of mycorrhizal fungi on whole-plant nutrient economics. *Proc. Natl. Acad. Sci. U.S.A.* **116**, 23163–23168 (2019).
13. J. J. Elser, W. F. Fagan, A. J. Kerkhoff, N. G. Swenson, B. J. Enquist, Biological stoichiometry of plant production: Metabolism, scaling and ecological response to global change. *New Phytol.* **186**, 593–608 (2010).
14. S. A. Sistla, J. P. Schimel, Stoichiometric flexibility as a regulator of carbon and nutrient cycling in terrestrial ecosystems under change. *New Phytol.* **196**, 68–78 (2012).
15. P. M. Vitousek, D. N. Menge, S. C. Reed, C. C. Cleveland, Biological nitrogen fixation: Rates, patterns and ecological controls in terrestrial ecosystems. *Philos. Trans. R. Soc. B: Biol. Sci.* **368**, 20130119 (2013).
16. C. C. Cleveland *et al.*, Exploring the role of cryptic nitrogen fixers in terrestrial ecosystems: A frontier in nitrogen cycling research. *Ecosystems* **25**, 1653–1669 (2022).
17. J. G. Canadell *et al.*, *2021: Global Carbon and Other Biogeochemical Cycles and Feedbacks* (Cambridge University Press, 2021).
18. V. K. Arora *et al.*, Carbon–concentration and carbon–climate feedbacks in CMIP6 models and their comparison to CMIP5 models. *Biogeosciences* **17**, 4173–4222 (2020).
19. W. R. Wieder, C. C. Cleveland, W. K. Smith, K. Todd-Brown, Future productivity and carbon storage limited by terrestrial nutrient availability. *Nat. Geosci.* **8**, 441–444 (2015).
20. T. Davies-Barnard *et al.*, Nitrogen cycling in CMIP6 land surface models: Progress and limitations. *Biogeosciences* **17**, 5129–5148 (2020).
21. T. Davies-Barnard, S. Zaehle, P. Friedlingstein, Assessment of the impacts of biological nitrogen fixation structural uncertainty in CMIP6 earth system models. *Biogeosciences* **19**, 3491–3503 (2022).
22. B. D. Stocker *et al.*, Terrestrial nitrogen cycling in Earth system models revisited. *New Phytol.* **210**, 1165–1168 (2016).
23. C. C. Cleveland *et al.*, Global patterns of terrestrial biological nitrogen (N_2) fixation in natural ecosystems. *Glob. Biochem. Cycles* **13**, 623–645 (1999).
24. V. P. Gutschick, Evolved strategies in nitrogen acquisition by plants. *Am. Nat.* **118**, 607–637 (1981).
25. J. B. Fisher *et al.*, Carbon cost of plant nitrogen acquisition: A mechanistic, globally applicable model of plant nitrogen uptake, retranslocation, and fixation. *Glob. Biogeochem. Cycles* **24**, 1–17 (2010).
26. C. R. Reis Ely *et al.*, Global terrestrial nitrogen fixation and its modification by agriculture. *Nature* **643**, 705–711 (2025).
27. S. Kou-Giesbrecht, V. K. Arora, Representing the dynamic response of vegetation to nitrogen limitation via biological nitrogen fixation in the CLASSIC land model. *Glob. Biogeochem. Cycles* **36**, e2022GB007341 (2022).
28. W. R. Wieder, C. C. Cleveland, D. M. Lawrence, G. B. Bonan, Effects of model structural uncertainty on carbon cycle projections: Biological nitrogen fixation as a case study. *Environ. Res. Lett.* **10**, 044016 (2015).
29. G. C. Hurtt *et al.*, Harmonization of global land use change and management for the period 850–2100 (LUH2) for CMIP6. *Geosci. Model Dev.* **13**, 5425–5464 (2020).
30. J. T. Abatzoglou, S. Z. Dobrowski, S. A. Parks, K. C. Hegewisch, TerraClimate, a high-resolution global dataset of monthly climate and climatic water balance from 1958–2015. *Sci. Data* **5**, 170191 (2018).
31. S. W. Running, M. Zhao, MODIS/terra net primary production gap-filled yearly L4 global 500m SIN grid V061. NASA EOSDIS Land Processes Distributed Active Archive Center. https://doi.org/10.5067/MODIS/MOD17A3HGF.061. Accessed 28 April 2023.
32. C. Gong, S. Kou-Giesbrecht, S. Zaehle, Anthropogenic-driven perturbations on nitrogen cycles and interactions with climate changes. *Curr. Opin. Green Sustainable Chem.* **46**, 100897 (2024), 10.1016/j.cogsc.2024.100897.

33. H. Tian *et al.*, Global nitrous oxide budget (1980–2020). *Earth Syst. Sci. Data* **16**, 2543–2604 (2024).
34. L. F. Schulte-Uebbing, A. H. W. Beusen, A. F. Bouwman, W. de Vries, From planetary to regional boundaries for agricultural nitrogen pollution. *Nature* **610**, 507–512 (2022).
35. M. A. Friedl *et al.*, MODIS collection 5 global land cover: Algorithm refinements and characterization of new datasets. *Remote Sens. Environ.* **114**, 168–182 (2010).
36. M. Jung *et al.*, Scaling carbon fluxes from eddy covariance sites to globe: Synthesis and evaluation of the FLUXCOM approach. *Biogeosciences* **17**, 1343–1365 (2020).
37. W. R. Wieder *et al.*, Beyond static benchmarking: Using experimental manipulations to evaluate land model assumptions. *Glob. Biogeochem. Cycles* **33**, 1289–1309 (2019).
38. M. E. Dusenge, A. G. Duarte, D. A. Way, Plant carbon metabolism and climate change: Elevated CO_2 and temperature impacts on photosynthesis, photorespiration and respiration. *New Phytol.* **221**, 32–49 (2019).
39. A. P. Walker *et al.*, Integrating the evidence for a terrestrial carbon sink caused by increasing atmospheric CO_2. *New Phytol.* **229**, 2413–2445 (2020).
40. J. K. Ladha *et al.*, Biological nitrogen fixation and prospects for ecological intensification in cereal-based cropping systems. *Field Crops Res.* **283**, 108541 (2022).
41. S. F. Hupperts, S. Gerber, M.-C. Nilsson, M. J. Gundale, Empirical and Earth system model estimates of boreal nitrogen fixation often differ: A pathway toward reconciliation. *Glob. Change Biol.* **27**, 5711–5725 (2021).
42. T. A. Bytnerowicz, P. Akana, K. Griffin, D. N. L. Menge, The temperature sensitivity of woody dinitrogen fixation across species and growing temperatures. *Nat. Plants* **8**, 209–216 (2022).
43. S. Kou-Giesbrecht *et al.*, Evaluating nitrogen cycling in terrestrial biosphere models: A disconnect between the carbon and nitrogen cycles. *Earth Syst. Dyn.* **14**, 767–795 (2023).
44. D. N. L. Menge, A. A. Wolf, J. L. Funk, Diversity of nitrogen fixation strategies in Mediterranean legumes. *Nat. Plants* **1**, 1–5 (2015).
45. T. Yu, Q. Zhuang, Modeling biological nitrogen fixation in global natural terrestrial ecosystems. *Biogeosciences* **17**, 3643–3657 (2020).
46. J. Peng *et al.*, Global carbon sequestration is highly sensitive to model-based formulations of nitrogen fixation. *Glob. Biogeochem. Cycles* **34**, e2019GB006296 (2020).
47. M. Zheng *et al.*, Effects of human disturbance activities and environmental change factors on terrestrial nitrogen fixation. *Glob. Change Biol.* **26**, 6203–6217 (2020).
48. S. Kou-Giesbrecht *et al.*, Rising nitrogen deposition leads to only a minor increase in CO_2 uptake in Earth system models. *Commun. Earth Environ.* **6**, 216 (2025).
49. M. Zheng, Z. Zhou, Y. Luo, P. Zhao, J. Mo, Global pattern and controls of biological nitrogen fixation under nutrient enrichment: A meta-analysis. *Glob. Change Biol.* **25**, 3018–3030 (2019).
50. S. A. Batterman, N. Wurzburger, L. O. Hedin, Nitrogen and phosphorus interact to control tropical symbiotic N_2 fixation: A test in *inga punctata*. *J. Ecol.* **101**, 1400–1408 (2013).
51. A. Hall, P. Cox, C. Huntingford, S. Klein, Progressing emergent constraints on future climate change. *Nat. Clim. Change* **9**, 269–278 (2019).
52. T. F. Keenan *et al.*, A constraint on historic growth in global photosynthesis due to rising CO_2. *Nat. Clim. Change* **13**, 1376–1381 (2023).
53. C. R. Reis Ely *et al.*, Global gridded dataset of terrestrial biological nitrogen fixation across natural and agricultural biomes: U.S. Geological Survey data release. https://doi.org/10.5066/P13THKNR. Deposited 2025. Accessed 14 April 2025.
54. C. R. Reis Ely *et al.*, A global dataset of terrestrial biological nitrogen fixation: U.S. Geological Survey data release. https://doi.org/10.5066/P1MFBVHK. Deposited 2025. Accessed 14 April 2025.
55. J. Liang, X. Qi, L. Souza, Y. Luo, Processes regulating progressive nitrogen limitation under elevated carbon dioxide: A meta-analysis. *Biogeosciences* **13**, 2689–2699 (2016).
56. X. Lan, P. Tans, K. W. Thoning, Trends in globally-averaged CO_2 determined from NOAA Global Monitoring Laboratory measurements. https://doi.org/10.15138/9N0H-ZH07. Accessed 28 April 2023.
57. L. V. Hedges, J. Gurevitch, P. S. Curtis, The meta-analysis of response ratios in experimental ecology. *Ecology* **80**, 1150–1156 (1999).
58. W. Viechtbauer, Conducting meta-analyses in R with the metafor package. *J. Stat. Softw.* **36**, 1–48 (2010).
59. P. Potapov *et al.*, Global maps of cropland extent and change show accelerated cropland expansion in the twenty-first century. *Nat. Food* **3**, 19–28 (2022).
60. S. Wenzel, P. M. Cox, V. Eyring, P. Friedlingstein, Projected land photosynthesis constrained by changes in the seasonal cycle of atmospheric CO_2. *Nature* **538**, 499–501 (2016).
61. C. Seiler *et al.*, Are terrestrial biosphere models fit for simulating the global land carbon sink? *J. Adv. Model. Earth Syst.* **14**, e2021MS002946 (2022).
62. P. M. Cox *et al.*, Emergent constraints on carbon budgets as a function of global warming. *Nat. Commun.* **15**, 1885 (2024).
63. R. J. Hijmans, terra: Spatial data analysis. R package version 1.8-70. https://CRAN.R-project.org/package=terra. Accessed 24 April 2023.
64. R Core Team, *R: A Language and Environment for Statistical Computing* (R Core Team, 2025).